Supplemental Material
Universality of the nonphononic vibrational spectrum across different classes of computer glasses

David Richard,[1] Karina González-López,[1] Geert Kapteijns,[1] Robert Pater,[1] Talya Vaknin,[2] Eran Bouchbinder,[2] and Edan Lerner[1]

[1] *Institute for Theoretical Physics, University of Amsterdam, Science Park 904, 1098 XH Amsterdam, The Netherlands*

[2] *Chemical and Biological Physics Department, Weizmann Institute of Science, Rehovot 7610001, Israel*

In this Supplemental Material we provide detailed descriptions of the computer models employed in our work, and the protocol used to prepare our ensembles of glassy samples. For each model we specify its associated microscopic units; however, we reiterate that in the main text we express frequencies in terms of c_s/a_0 where $a_0 \equiv (V/N)^{1/3}$ is a microscopic length, $c_s \equiv \sqrt{G/\rho}$ is the speed of shear waves, G denotes the athermal shear modulus [1], ρ is the mass density, $V = L^3$ is the volume, and N is the number of particles. For all models, the low-frequency spectra is extracted via a partial diagonalization using the ARPACK package [2].

S-1. Elastic spheres

We employ a simple-yet-realistic model of soft, linear-elastic spheres interacting via the Hertzian interaction law [3]

$$\varphi_{\rm Hertz}(r) = \tfrac{2\varepsilon}{5}\big(r - \tfrac{\sigma_i+\sigma_j}{2}\big)^{5/2}\Theta\big(\tfrac{\sigma_i+\sigma_j}{2} - r\big)\,, \qquad \text{(S1)}$$

where σ_i, σ_j denote the radii of the $i^{\rm th}$ and $j^{\rm th}$ particles, and $\Theta(x)$ is the Heaviside step function. We enclose $N = 32000$ particles of equal mass m in a box of volume $V = L^3$, and fix the number density at $N/V = 0.9386$. We choose 50% of particles to have $\sigma_i = 0.5$ and the other 50% to have $\sigma_i = 0.7$. Length are expressed in terms of the diameter of the smaller species, and energies in terms of ε.

To make glassy samples of elastic spheres, we first equilibrate the liquid phase at $T = 0.004/k_B$ (here the computer $T_g \approx 0.0017/k_B$), and follow the equilibration with an instantaneous quench using a nonlinear conjugate gradient algorithm [4] to form a glass. Following this protocol, we created and analyzed an ensemble of 1300 independent glassy samples, whose pressure-to-bulk modulus ratio is $p/K \approx 0.173$.

S-2. Stillinger-Weber network glass

Originally developed to model silicon [5], the Stillinger-Weber (SW) potential has become widely used to model the phase behavior of tetrahedral liquids, from investigating liquid-liquid phase separation [6], to ice nucleation [7]. This model and its dynamics and thermodynamics are widespread in the literature; here we nevertheless spell out the potential energy $U_{\rm SW}$ definition, followed by expressions for its Hessian matrix $\boldsymbol{\mathcal{M}}_{mn} \equiv \frac{\partial^2 U_{\rm SW}}{\partial \boldsymbol{x}_m \partial \boldsymbol{x}_n}$, which, to the best of our knowledge, is not available in the current literature.

The SW model is a monocomponent system of N identical particles of mass m whose interaction potential consists of both a short-ranged, two-body interaction

$$\varphi_2(r_{ij}) = A\varepsilon\left(\frac{B\sigma^4}{r_{ij}^4} - 1\right)\exp\left(\frac{\sigma}{r_{ij} - r_c}\right), \qquad \text{(S2)}$$

and a three-body term

$$\varphi_3(r_{ij}, r_{ik}, \theta_{jik}) = \lambda\varepsilon\left(\cos\theta_{jik} - \cos\theta_0\right)^2 \times \exp\left(\frac{\gamma\sigma}{r_{ij} - r_c}\right)\exp\left(\frac{\gamma\sigma}{r_{ik} - r_c}\right), \qquad \text{(S3)}$$

that favors triplets of atoms to form an angle $\theta_0 \simeq 109^{\rm o}$. Here θ_{jik} is the angle formed by the i,j and i,k bonds, $r_{ij} \equiv |\boldsymbol{x}_{ij}|$ is the pairwise distance between particles i and j (with $\boldsymbol{x}_{ij} \equiv \boldsymbol{x}_j - \boldsymbol{x}_i$), r_c is a cutoff distance, A, B, λ and γ are dimensionless parameters, and σ, ε are microscopic length and energy scales, respectively. The total potential energy of the system is computed as

$$U_{\rm SW} = \sum_i \sum_{j>i} \varphi_2(r_{ij}) + \sum_i \sum_{j\neq i} \sum_{k>j} \varphi_3(r_{ij}, r_{ik}, \theta_{jik}). \qquad \text{(S4)}$$

We chose all microscopic parameters (A, B, γ, r_c) to be the same as in the SW parametrization of silicon [5], except for λ — whose high values favor local tetragonal order — which was set to 18.75. This value is found optimal to achieve good glass forming ability [8]. Lengths are expressed in terms of σ, and energies in terms of ε. Simulations are performed in the NVT ensemble using the highly parallel LAMMPS package [9]. The temperature is controlled using the Nosé-Hoover thermostat, the number density is set to $N/V = 0.52\sigma^{-3}$ and the temperature is fixed to $T = 0.1\varepsilon/k_B$, which is far above our estimate for the glass transition temperature $T_g \approx 0.014\varepsilon/k_B$.

To prepare glassy states, we collect a set of uncorrelated equilibrium configurations and perform an instan-

taneous quench of each configuration by minimizing the potential energy using a nonlinear conjugate gradient algorithm [4]. With this protocol, we gathered 1300 independent glassy samples, each composed of $N = 4096$ particles.

Expressions for the Hessian matrix

For ease of notation in spelling out the expression for the Hessian matrix $\boldsymbol{\mathcal{M}}_{mn} \equiv \frac{\partial^2 U_{\rm SW}}{\partial \boldsymbol{x}_m \partial \boldsymbol{x}_n}$, we denote pairs of particles with Greek indices, e.g. $r_{ij} \equiv r_\alpha$, then the potential energy can be spelled out as

$$U_{\rm SW} = \sum_\alpha \varphi_2(r_\alpha) + \sum_{\alpha,\beta} \varphi_3(r_\alpha, r_\beta, \theta_{\alpha\beta}), \tag{S5}$$

where the sum over α, β runs over couples of pairs of particles that form a triple by sharing a common particle (e.g. i, j and i, k where $j \neq k$), and $\theta_{\alpha\beta}$ is the angle formed between $\boldsymbol{x}_\alpha$ and $\boldsymbol{x}_\beta$.

With these notations the Hessian matrix can be decomposed into a two-body part

$$\boldsymbol{\mathcal{M}}^{\rm 2body}_{mn} = \sum_\alpha \Gamma_{mn\alpha} \left(\frac{\mathcal{I} - \hat{\boldsymbol{x}}_\alpha \hat{\boldsymbol{x}}_\alpha}{r_\alpha} \frac{\partial \varphi_2}{\partial r_\alpha} + \hat{\boldsymbol{x}}_\alpha \hat{\boldsymbol{x}}_\alpha \frac{\partial^2 \varphi_2}{\partial r_\alpha^2} \right), \tag{S6}$$

and a three-body part

$$\boldsymbol{\mathcal{M}}^{\rm 3body}_{mn} = \sum_{\alpha,\beta} \left(\Gamma_{mn\beta} \mathcal{D}_{\beta,\alpha} + \Gamma_{mn\alpha} \mathcal{D}_{\alpha,\beta} + \Gamma_{n\alpha}\Gamma_{m\beta} \mathcal{X}_{\alpha,\beta} + \Gamma_{n\beta}\Gamma_{m\alpha} \mathcal{X}_{\beta,\alpha} \right), \tag{S7}$$

where $\mathcal{I}$ is the identity tensor, $\Gamma_{m\alpha} \equiv (\delta_{jm} - \delta_{im})$, $\Gamma_{mn\alpha} \equiv (\delta_{jm} - \delta_{im})(\delta_{jn} - \delta_{in})$, and using the notation $c_{\alpha\beta} \equiv \cos\theta_{\alpha\beta}$, $\mathcal{D}_{\beta,\beta}$ and $\mathcal{X}_{\alpha,\beta}$ read

$$\mathcal{D}_{\alpha,\beta} \equiv \frac{\mathcal{I} - \hat{\boldsymbol{x}}_\alpha \hat{\boldsymbol{x}}_\alpha}{r_\alpha} \frac{\partial \varphi_3}{\partial r_\alpha} + \hat{\boldsymbol{x}}_\alpha \hat{\boldsymbol{x}}_\alpha \frac{\partial^2 \varphi_3}{\partial r_\alpha^2} + \frac{\partial^2 c_{\alpha\beta}}{\partial \boldsymbol{x}_\alpha \partial \boldsymbol{x}_\alpha} \frac{\partial \varphi_3}{\partial c_{\alpha\beta}} + \frac{\partial c_{\alpha\beta}}{\partial \boldsymbol{x}_\alpha} \frac{\partial c_{\alpha\beta}}{\partial \boldsymbol{x}_\alpha} \frac{\partial^2 \varphi_3}{\partial c_{\alpha\beta}^2} + \left(\hat{\boldsymbol{x}}_\alpha \frac{\partial c_{\alpha\beta}}{\partial \boldsymbol{x}_\alpha} + \frac{\partial c_{\alpha\beta}}{\partial \boldsymbol{x}_\alpha} \hat{\boldsymbol{x}}_\alpha \right) \frac{\partial^2 \varphi_3}{\partial r_\alpha \partial c_{\alpha\beta}}, \tag{S8}$$

and

$$\mathcal{X}_{\alpha,\beta} \equiv \hat{\boldsymbol{x}}_\alpha \hat{\boldsymbol{x}}_\beta \frac{\partial^2 \varphi_3}{\partial r_\alpha \partial r_\beta} + \frac{\partial c_{\alpha\beta}}{\partial \boldsymbol{x}_\alpha} \hat{\boldsymbol{x}}_\beta \frac{\partial^2 \varphi_3}{\partial r_\beta \partial c_{\alpha\beta}} + \frac{\partial^2 c_{\alpha\beta}}{\partial \boldsymbol{x}_\alpha \partial \boldsymbol{x}_\beta} \frac{\partial \varphi_3}{\partial c_{\alpha\beta}} + \frac{\partial c_{\alpha\beta}}{\partial \boldsymbol{x}_\alpha} \frac{\partial c_{\alpha\beta}}{\partial \boldsymbol{x}_\beta} \frac{\partial^2 \varphi_3}{\partial c_{\alpha\beta}^2} + \hat{\boldsymbol{x}}_\alpha \frac{\partial c_{\alpha\beta}}{\partial \boldsymbol{x}_\beta} \frac{\partial^2 \varphi_3}{\partial r_\alpha \partial c_{\alpha\beta}}, \tag{S9}$$

respectively. Furthermore

$$\frac{\partial c_{\alpha\beta}}{\partial \boldsymbol{x}_\alpha} = \frac{\hat{\boldsymbol{x}}_\beta - \hat{\boldsymbol{x}}_\alpha c_{\alpha\beta}}{r_\alpha}, \tag{S10}$$

$$\frac{\partial^2 c_{\alpha\beta}}{\partial \boldsymbol{x}_\alpha \partial \boldsymbol{x}_\alpha} = \frac{1}{r_\alpha^2} \left((3\hat{\boldsymbol{x}}_\alpha \hat{\boldsymbol{x}}_\alpha - \mathcal{I})\, c_{\alpha\beta} - (\hat{\boldsymbol{x}}_\alpha \hat{\boldsymbol{x}}_\beta + \hat{\boldsymbol{x}}_\beta \hat{\boldsymbol{x}}_\alpha) \right), \tag{S11}$$

and

$$\frac{\partial^2 c_{\alpha\beta}}{\partial \boldsymbol{x}_\alpha \partial \boldsymbol{x}_\beta} = \frac{1}{r_\alpha r_\beta} \left(\mathcal{I} - \hat{\boldsymbol{x}}_\alpha \hat{\boldsymbol{x}}_\alpha - \hat{\boldsymbol{x}}_\beta \hat{\boldsymbol{x}}_\beta + \hat{\boldsymbol{x}}_\alpha \hat{\boldsymbol{x}}_\beta c_{\alpha\beta} \right) \tag{S12}$$

The implementation of the Hessian was validated using finite differences.

S-3. Molecular glass

The well-known model by Lewis-Wahnström [10] for the fragile glass former ortho-terphenyl (OTP) describes the OTP molecule as a rigid triangular molecule with site interactions at each vertex of the triangle, where each of these sites represents a whole phenyl ring that interacts with sites of different molecules via a Lennard-Jones potential. Inspired by this description, we consider a system of N_m molecules comprised of $N = 3N_m$ particles in three dimensions. We model the OTP molecule as a three-site isosceles triangle with two sides of length σ, and an angle between them of 75°. The intermolecular (site-site) interactions are given by the same smoothed Lennard Jones pairwise potential $\varphi_{\rm LJ}$ as employed in the polymer system, see Eq. (S16). Lengths and energies are expressed in terms of σ and ε, respectively.

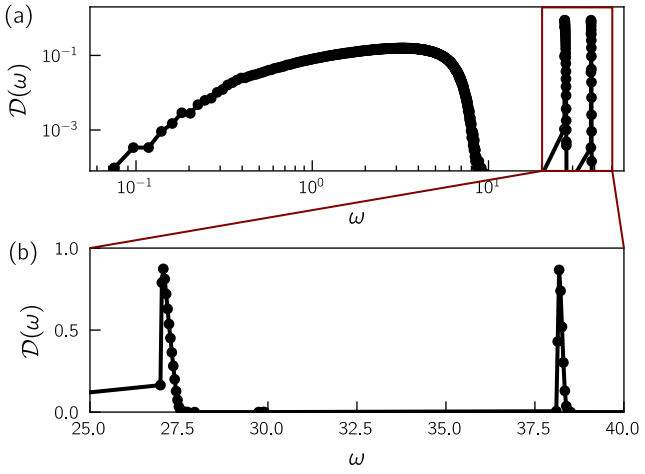

FIG. S1. (a) Full density of states of the OTP model with $N = 3000$. (b) Zoom on the two peaks associated to the intra-molecular vibrational modes.

In contrast to [10], in our model the three sites within a single molecule interact via a stiff harmonic potential, that reads:

$$\varphi_{\rm bonds} = \tfrac{1}{2} k (r_{ij} - l_0)^2, \tag{S13}$$

where r_{ij} is the distance between the $i^{\rm th}$ and $j^{\rm th}$ atoms in a molecule, l_0 represents the rest length of the intramolecular bonds, and $k = 5{\times}10^3 \varepsilon/\sigma^2$ denotes the stiffness of the

intramolecular bonds, chosen to be roughly two orders of magnitude higher than typical intermolecular stiffnesses.

Glassy samples are prepared with the same method as employed in the polymeric system. We equilibrate our system in the NVT ensemble at a number density $N/V = 0.80\sigma^{-3}$ and a temperature $T = 4.0\varepsilon/k_B$. Uncorrelated equilibrium configurations are prepared using conventional molecular dynamics and a Berendsen thermostat [11], for which we set the time constant to $\tau_{_T} = 1.0\sqrt{m\sigma^2/\varepsilon}$. After equilibration, an instantaneous quench to zero temperature using a conjugate gradient algorithm is performed. With this procedure we generate 5000 independent glassy samples of $N_m = 3000$ molecules that contains $N = 9000$ atoms. In Fig. S1, we provide the full density of states of the OTP system.

S-4. Polymer glass

Polymer melts are usually coarse-grained via simple bead-spring models where the actual monomer chemistry is replaced by an effective bead. Probably the most famous, the Kremer-Grest Model describes a polymeric chain via the finite extensible nonlinear elastic (FENE) potential [12]. In this work, we adopt the same modeling expect that we replace the original repulsive Weeks-Chandler-Andersen potential [13] with a smoothed inverse-power law pairwise potential

$$\varphi_{\text{IPL}}(r_{ij}) = \begin{cases} \varepsilon\left[\left(\frac{\lambda}{r_{ij}}\right)^{10} + \sum_{\ell=0}^{3} c_{2\ell}\left(\frac{r_{ij}}{\lambda}\right)^{2\ell}\right] & , \; r_{ij} \le r_c^{\text{IPL}} \\ 0 & , \; r_{ij} \ge r_c^{\text{IPL}} \end{cases}, \tag{S14}$$

where λ is a microscopic length to be specified in what follows, and the coefficients $c_{2\ell}$ are determined by demanding that φ_{IPL} vanishes continuously up to three derivatives at the cutoff r_c^{IPL}, see e.g. [14].

The full modified FENE (mFENE) potential for nearest bonded monomers reads

$$\varphi_{\text{mFENE}}(r_{ij}) = \varphi_{\text{IPL}}(r_{ij}) - \tfrac{1}{2}\kappa l_0^2 \ln\left(1 - (r_{ij}/l_0)^2\right). \tag{S15}$$

Non-bonded intramolecular monomers only interact via φ_{IPL} to account for volume exclusion. Intermolecular monomers interactions are given by a smoothed Lennard Jones pairwise potential (see e.g. [15]) of the form:

$$\varphi_{\text{LJ}}(r_{ij}) = \begin{cases} 6\varepsilon\left[\left(\frac{\sigma}{r_{ij}}\right)^{12} - \left(\frac{\sigma}{r_{ij}}\right)^{6} + \sum_{l=0}^{3} c_{2l}\left(\frac{r_{ij}}{\sigma}\right)^{2l}\right], & r_{ij} < r_c^{\text{LJ}}, \\ 0, & r_{ij} \ge r_c^{\text{LJ}}, \end{cases} \tag{S16}$$

where r_{ij} is the distance between the i^{th} and j^{th} particles, ε is microscopic energy scale, σ is a microscopic length scale, and the coefficients c_{2l} are determined by requiring that three derivatives of φ_{LJ} with respect to r_{ij} vanish continuously at the cutoff $r_c^{\text{LJ}} = 2\sigma$ in the same manner as done for φ_{IPL}. In practice, we set $\lambda = 1.2\sigma$, $r_c^{\text{IPL}} = 1.776\sigma$, $l_0 = 1.5\sigma$, and $\kappa = 30.0\varepsilon/\sigma^2$.

To prepare the glassy samples, we first equilibrate the system in the NVT ensemble at a number density $N/V = 0.80\sigma^{-3}$ and a temperature $T = 4.0\varepsilon/k_B$, the latter residing far above the glass transition temperature. To this aim we used molecular dynamics and we employed the Berendsen thermostat [11], for which we set the time constant to $\tau_{_T} = 1.0\sqrt{m\sigma^2/\varepsilon}$. After equilibration, the energy is minimized instantaneously using a standard conjugate gradient algorithm. Following this procedure, we generated 5000 independent glassy samples of $N_c = 900$ chains composed of 10 monomers for a total of $N = 9000$ particles.

S-5. CuZr bulk metallic glass (BMG)

BMGs are simulated through the Embedded Atom Method (EAM) [16–18] in which the potential energy for atom i is given by

$$E_i^{\text{BMG}} = F_\alpha\left(\sum_{j\neq i} \rho_\beta(r_{ij})\right) + \frac{1}{2}\sum_{j\neq i} \phi_{\alpha\beta}(r_{ij}) \; , \tag{S17}$$

where the summations are over neighboring atoms j within a cutoff, and α and β are the element types of atoms i and j respectively. The values of the embedding function F_α, the pair potential function ϕ and the effective charge density ρ_β are derived from *ab initio* calculations as well as from experimental data, and are provided in [18].

We prepared glassy samples with 8000 atoms out of which 46% are Copper (Cu) and 54% Zirconium (Zr). The number density is set to $N/V = 0.058\mathring{A}^{-3}$ and the atom masses are set to their experimental values 91.22 grams/mole for Zirconium and 63.54 grams/mole for Copper. We equilibrate the liquid phase at 1500K and instantaneously quench by a conjugate-gradient algorithm. Our ensemble consists of 2086 samples with a shear modulus mean of 21.0GPa. Simulations are performed in the NVT ensemble using the highly parallel LAMMPS package [9].

The Hessian matrix for this model was calculated by moving each atom an infinitesimal distance Δ in each direction x, y and z and then measuring the change in forces $\boldsymbol{\mathcal{F}}$ on the atoms in the system. Following

$$\boldsymbol{\mathcal{M}} \cdot \boldsymbol{x} = -\boldsymbol{\mathcal{F}} \; , \tag{S18}$$

with e.g. $\boldsymbol{x} = \Delta\hat{\boldsymbol{x}}$, for a displacement in the x direction. We read out $\boldsymbol{\mathcal{M}}$ by normalizing the forces by the infinitesimal distance Δ.

S-6. History dependence of glass properties

Dimensionless observables that describe the core-size of quasilocalized modes and their density are the scaled

participation ratio Ne_0 and the prefactor $\mathcal{A}_g$ of the vDOS, respectively, measured and plotted for our studied computer glass models in Fig. 3 of the main text. As shown in Ref. [19], and also in Fig. S2 of this Supplemental Material, these quantities can depend on the protocol used to prepare glassy samples, here the parent temperature T_p from which the liquid is initially equilibrated before it is instantaneously quenched to $T = 0$. Fig. S2a, in particular, shows that $\mathcal{A}_g$ plateaus at high T_p (poorly annealed glasses) before it starts decreasing at low T_p. As seen here and also in [19], the decrease in $\mathcal{A}_g$ occurs in the close vicinity of (about 20%-30% above) the computer (MD) glass transition temperature.

In this work we are interested in comparing elastic properties of several classes of glass models. We therefore focus our investigation on the high-parent-temperature regime, i.e. far above these models' respective computer glass transition temperatures, where elastic properties become independent of parent temperature. This allows us to meaningfully compare these dimensionless observables across the different classes of glasses.

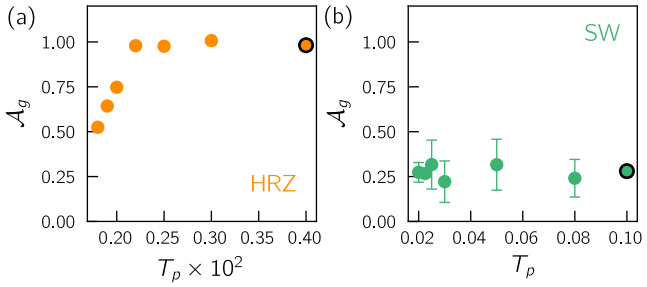

FIG. S2. Dimensionless prefactor of the vibrational density of states for the Hertzian (a) and Stillinger-Weber (b) models, plotted as a function of the parent temperature T_p. The parent temperature that represents the data shown in the main text is indicated by a black edge.

[1] J. F. Lutsko, Generalized expressions for the calculation of elastic constants by computer simulation, J. Appl. Phys. **65**, 2991 (1989).

[2] R. B. Lehoucq, D. C. Sorensen, and C. Yang, *ARPACK Users' Guide* (Society for Industrial and Applied Mathematics, Philadelphia, 1998).

[3] H. R. Hertz, *Über die Berührung fester elastischer Körper und über die Härte* (Universitätsbibliothek Johann Christian Senckenberg, 2006).

[4] D. MacKay, macopt optimizer (2004).

[5] F. H. Stillinger and T. A. Weber, Computer simulation of local order in condensed phases of silicon, Phys. Rev. B **31**, 5262 (1985).

[6] V. V. Vasisht, S. Saw, and S. Sastry, Liquid–liquid critical point in supercooled silicon, Nat. Phys. **7**, 549 (2011).

[7] T. Li, D. Donadio, G. Russo, and G. Galli, Homogeneous ice nucleation from supercooled water, Phys. Chem. Chem. Phys. **13**, 19807 (2011).

[8] J. Russo, F. Romano, and H. Tanaka, Glass forming ability in systems with competing orderings, Phys. Rev. X **8**, 021040 (2018).

[9] S. Plimpton, *Fast parallel algorithms for short-range molecular dynamics*, Tech. Rep. (Sandia National Labs., Albuquerque, NM (United States), 1993).

[10] L. J. Lewis and G. Wahnström, Relaxation of a molecular glass at intermediate times, Solid State Commun. **86**, 295 (1993).

[11] H. J. C. Berendsen, J. P. M. Postma, W. F. van Gunsteren, A. DiNola, and J. R. Haak, Molecular dynamics with coupling to an external bath, J. Chem. Phys. **81**, 3684 (1984).

[12] K. Kremer and G. S. Grest, Dynamics of entangled linear polymer melts: a moleculardynamics simulation, J. Chem. Phys. **92**, 5057 (1990).

[13] J. D. Weeks, D. Chandler, and H. C. Andersen, Role of repulsive forces in determining the equilibrium structure of simple liquids, J. Chem. Phys. **54**, 5237 (1971).

[14] E. Lerner and E. Bouchbinder, A characteristic energy scale in glasses, J. Chem. Phys. **148**, 214502 (2018).

[15] G. Kapteijns, W. Ji, C. Brito, M. Wyart, and E. Lerner, Fast generation of ultrastable computer glasses by minimization of an augmented potential energy, Phys. Rev. E **99**, 012106 (2019).

[16] Y. Q. Cheng, E. Ma, and H. W. Sheng, Atomic level structure in multicomponent bulk metallic glass, Phys. Rev. Lett. **102**, 245501 (2009).

[17] Y. Cheng and E. Ma, Atomic-level structure and structure–property relationship in metallic glasses, Prog. Mater. Sci. **56**, 379 (2011).

[18] Cu-zr eam potential (2011).

[19] C. Rainone, E. Bouchbinder, and E. Lerner, Pinching a glass reveals key properties of its soft spots, Proc. Natl. Acad. Sci. U.S.A. **117**, 5228 (2020).